Atmospheric Environment 267 (2021) 118748

Contents lists available at ScienceDirect

Atmospheric Environment

journal homepage: www.elsevier.com/locate/atmosenv

Relationship between cloud condensation nuclei (CCN) concentration and aerosol optical depth in the Arctic region

Seo H. Ahn [a,b], Y.J. Yoon [a], T.J. Choi [a], J.Y. Lee [c], Y.P. Kim [d], B.Y. Lee [a], C. Ritter [e], W. Aas [f], R. Krejci [g], J. Ström [g], P. Tunved [g], Chang H. Jung [h,*]

[a] Korea Polar Research Institute (KOPRI), 26 Songdomirae-ro, Yeonsu-gu, Incheon, 21990, Republic of Korea
[b] University of Science and Technology, 217 Gajeong-ro, Yuseong-gu, Daejeon, 34113, Republic of Korea
[c] Department of Environmental Science and Engineering, Ewha Womans University, Seoul, 03760, Republic of Korea
[d] Department of Chemical Engineering and Materials Science, Ewha Womans University, Seoul, 03760, Republic of Korea
[e] Alfred-Wegener-Institut, Helmholtz-Zentrum für Polar- und Meeresforschung, Telegrafenberg A45, 14473, Potsdam, Germany
[f] NILU – Norwegian Institute for Air Research, Kjeller, 2027, Norway
[g] Department of Environmental Science & Bolin Centre for Climate Research, Stockholm University, S 106 91 Stockholm, Sweden
[h] Department of Health Management, Kyungin Women's University, Incheon, 21041, Republic of Korea

HIGHLIGHTS

- Relationship between CCN concentration and AOD was parameterized with statistically significant.
- AOD from MERRA-2 and MODIS were comparable with ground-based measurements of AOD.
- In-situ aerosol optical properties reproduce the CCN most efficiently.

ARTICLE INFO

Keywords:
Arctic region
Cloud condensation nuclei
Aerosol optical depth
CCN–AOD relationship
Black carbon

ABSTRACT

To determine the direct and indirect effects of aerosols on climate, it is important to know the spatial and temporal variations in cloud condensation nuclei (CCN) concentrations. Although many types of CCN measurements are available, extensive CCN measurements are challenging because of the complexity and high operating cost, especially in remote areas. As aerosol optical depth (AOD) can be readily observed by remote sensing, many attempts have been made to estimate CCN concentrations from AOD. In this study, the CCN–AOD relationship is parameterized based on CCN ground measurements from the Zeppelin Observatory (78.91° N, 11.89° E, 474 m asl) in the Arctic region. The AOD measurements were obtained from the Ny-Ålesund site (78.923° N, 11.928° E) and Modern-Era Retrospective Analysis for Research and Applications, Version 2 reanalysis. Our results show a CCN–AOD correlation with a coefficient of determination R^2 of 0.59. Three additional estimation models for CCN were presented based on the following data: (i) in situ aerosol chemical composition, (ii) in situ aerosol optical properties, and (iii) chemical composition of AOD obtained from reanalysis data. The results from the model using in situ aerosol optical properties reproduced the observed CCN concentration most efficiently, suggesting that the contribution of BC to CCN concentration should be considered along with that of sulfate.

1. Introduction

To better characterize the effects of aerosols on climate, particularly the indirect effects, cloud condensation nuclei (CCN) concentrations, and their spatial and temporal variations must be identified and quantified. Generally, CCN concentration is determined by the

Abbreviations: AE, Ångström Exponent; AERONET, Aerosol Robotic Network; BC, Black Carbon; CCN-AI, Aerosol Index; GOCART, Goddard Chemistry Aerosol Radiation and Transport; MERRA-2, Modern-Era Retrospective Analysis for Research and Applications, version 2; MODIS, Moderate Resolution Imaging Spectroradiometer Collection; PSAP, Particle Soot Absorption Photometer; SS, Supersaturation.

* Corresponding author. Kyungin Women's University, 63 Gyeyangsan-ro, Gyeyang-gu, Incheon, 21041, Republic of Korea.
E-mail address: jch@kiwu.ac.kr (C.H. Jung).

https://doi.org/10.1016/j.atmosenv.2021.118748
Received 2 January 2021; Received in revised form 14 September 2021; Accepted 21 September 2021
Available online 24 September 2021

environmental water vapor supersaturation associated with humidity and temperature, as well as the aerosol size distribution, chemical composition, and the aerosol concentration within the lower troposphere (Pierce and Adams, 2009; Liu and Li, 2014). Measurement of the CCN concentration and size distribution of aerosol particles are relatively complicated compared to aerosol optical quantities. For example, aerosol optical depth (AOD) and aerosol scattering/extinction coefficients can be measured using ground-based and remote sensing instruments (Kapustin et al., 2006; Andreae, 2009; Liu and Li, 2014). In particular, remote sensing can help cover large areas in a short time. Aerosol optical properties can be availed from satellite measurements, the surface-based Aerosol Robotic Network (AERONET), and reanalysis data including the Modern-Era Retrospective Analysis for Research and Applications, version 2 (MERRA-2), and Copernicus Atmosphere Monitoring Service (CAMS) reanalysis dataset, which is an aerosol assimilation product from the European Centre for Medium-Range Weather Forecasts (ECMWF).

Several previous studies have demonstrated a correlation between CCN concentration and aerosol optical properties, such as AOD and extinction coefficient (Nakajima et al., 2001; Bréon et al., 2002; Feingold et al., 2003; Yuan et al., 2008; Andreae, 2009; Quaas et al., 2009; Shinozuka et al., 2009, 2015; Jefferson, 2010; Liu et al., 2011; Wang et al., 2011; Tao et al., 2012; Grandey et al., 2013). By comparing AERONET AOD with CCN measurements, Andreae (2009) found a correlation between AOD and CCN number concentration. Romakkaniemi et al. (2012) suggested that AOD can be used as a proxy for CCN. Liu et al. (2011) examined the relationship of CCN–AI (Aerosol Index) with the observation data collected from a polluted site in China using the Ångström exponent (AE) as a characterization of particle size. In addition, Koike et al. (2019) used the aerosol number–size distribution as a proxy for CCN and compared it with AI.

The studies mentioned above showed that using aerosol optical measurements to estimate CCN concentration is a scientifically sound approach. The use of extinction coefficients-CCN parameterizations to retrieve CCN from ground lidar systems has been demonstrated (Mamouri and Ansmann, 2016). Moreover, Georgoulias et al. (2020) were the first to retrieve CCN profiles from a satellite-based lidar, the Cloud-Aerosol Lidar with Orthogonal Polarization (CALIOP) instrument flown aboard the Cloud-Aerosol Lidar and Infrared Pathfinder Satellite Observation (CALIPSO) satellite, based on such parameterizations. However, there are challenges in using AOD as a proxy for CCN (Stier, 2016). Although AOD and CCN are related to CCN concentration and aerosol particle size distribution, uncertainties exist when using AOD as an indicator of CCN (Tang et al., 2014). CCN concentrations can vary for a given AOD, depending on regional characteristics, such as aerosol size distribution and meteorological conditions (e.g., relative humidity (RH)) (Romakkaniemi et al., 2012). Other aerosol intensive properties, such as refractive index, mixing state, particle shape, and surface tension, can also influence this relationship. Despite these limitations, a high correlation coefficient (0.98) was observed between the AOD and CCN (Andreae, 2009). Thus, the CCN–AOD relationship can be further understood by a detailed consideration of several physicochemical characteristics, such as chemically resolved aerosol characteristics and meteorological conditions, which can be represented as seasonal differences in addition to RH.

Compared with other regions, it is more challenging to obtain in-situ measurement data in the Arctic region. Studies involving the direct long-term measurements of CCN are sparse, and the study by Jung et al. (Tellus, 2018) provides the only available observational long-term CCN time series. Several studies have been conducted to estimate Arctic CCN concentrations (Ström et al., 2003, 2009; Engvall et al., 2008; Tunved et al., 2013) from aerosol measurements. Based on aerosol measurements near the Alaskan Arctic and the North American Arctic regions, it was suggested that most Arctic aerosols act as CCN above 0.1% supersaturation. Furthermore, the closure of CCN was assessed using measured size distributions, bulk chemical composition, and assumed aerosol mixing state; these CCN were overpredicted with the best accuracy reaching 20%–30% (Moore et al., 2011; Lathem et al., 2013). In addition, Zábori et al. (2015) presented CCN spectral parameters C and k using a power-law function fitted for CCN based on measurements at the Zeppelin station in June and August 2009. Herenz et al. (2018) discovered that the particle–number concentration at 3000 m was 20 times higher than those measured below 2000 m in some cases; furthermore, their size distributions were different. This indicates the long-range transport of aerosols from the lower latitudes into the Arctic through advection from different regions at different altitudes. Thus, in the Arctic region with little measurement data, AOD, which represents the optical attenuation by aerosols throughout an entire column of the atmosphere, may be used to estimate CCN.

In this study, the CCN–AOD relationship was investigated using ground-based and satellite measurements and reanalysis data in the Arctic region. First, trends in CCN concentration and AOD were determined from observations of CCN at the Zeppelin Observatory and measurements of AOD at Ny-Ålesund, along with Moderate Resolution Imaging Spectroradiometer Collection 6 (MODIS) and Modern-Era Retrospective Analysis for Research and Applications, Version 2 (MERRA-2) reanalysis data. Second, the relationship between CCN and AOD is investigated with respect to seasonality and linked to aerosol physical or optical properties, such as aerosol size or absorption information. Finally, multiple regression models are presented to estimate CCN concentration using aerosol chemical composition data, including total sulfate, black carbon, and chemically resolved aerosol optical properties.

2. Methodology

The procedure for the analysis in this study is as follows: Temporal variations in CCN and AOD for the Zeppelin station and their seasonal characteristics were investigated. The relationship between AOD and CCN was derived from linear regression analysis to estimate the CCN. Three additional CCN estimation models were presented with multiple regression analysis based on the following data: (i) in situ aerosol chemical composition data, which is sulfate concentration, (ii) in situ aerosol optical property data, which are scattering/absorption coefficients, and (iii) the chemical composition of AOD obtained from reanalysis data which are AOD_{SO4} and AOD_{BC}. The performance of each model was determined by comparing CCN derived from models and observed CCN at the Zeppelin station.

In situ CCN observations were carried out at the Zeppelin research station (78.91° N, 11.89° E, 474 m asl), located approximately 2 km southwest of the small settlement of Ny-Ålesund, Svalbard (Fig. 1). Continuous aerosol measurements at Zeppelin began in 2000. Previous studies have reported that new particle formation occurs not only at higher altitudes, including the free troposphere (Weber et al., 2003;

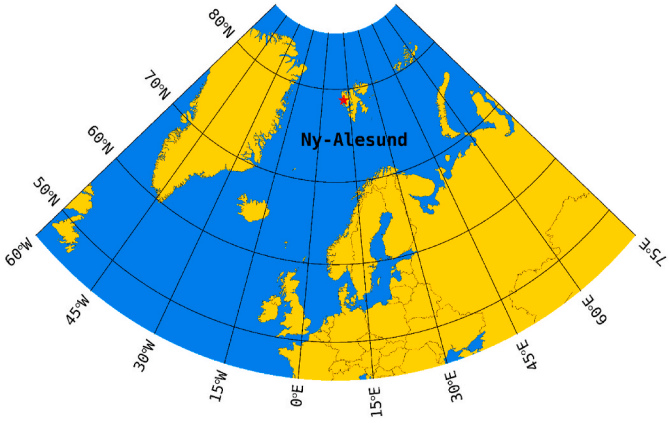

Fig. 1. Location of Ny-Ålesund, Svalbard.

Darani et al., 2010) but also in the boundary layer near the surface (Ström et al., 2009; Tunved et al., 2013; Jung et al., 2018). In this study, aerosol data were used to estimate CCN concentrations at the Zeppelin station from April 2007 to March 2013.

Aerosols play an important role in Earth's climate and hydrological cycle through their direct and indirect effects. Aerosols have direct radiative forcing because they scatter and absorb solar and infrared radiation in the atmosphere. Aerosols also change the formation and precipitation efficiency of clouds, thereby causing an indirect radiative forcing associated with these changes in cloud properties (Penner et al., 2001; Stocker, 2014). AOD is a measure of aerosols in an atmospheric vertical column and indicates the extinction of direct sunlight reaching Earth's surface. Aerosols are composed of various components such as sea salt, sulfate, and elemental carbon. Depending on their chemical and optical characteristics, they absorb or/and scatter solar radiation or can be activated to CCN, which are associated with the formation and persistence of clouds. Although AOD differs from CCN in that it does not directly depend on supersaturation and aerosol size distributions and represents the entire column of the atmosphere, CCN, governed by aerosol activity, also lead to solar radiation extinction. Therefore, there is an inevitable correlation between AOD and CCN.

However, the aerosol chemical composition is essential for defining the particle cloud nucleating ability (Kapustin et al., 2006). This is because the aerosol chemical composition can determine its size distributions and chemical properties, which is crucial for CCN formation. Sulfate particles are efficient for CCN activation owing to their chemical characteristics and size distributions (Boucher and Lohmann, 1995; Matsumoto et al., 1997), and long-range transport of anthropogenic aerosols can have an impact on CCN, especially in winter and spring in the Arctic. As per previous studies, black carbon (BC) increased markedly in the spring or winter, when CCN are high in the Arctic (Sharma et al., 2004; Gong et al., 2010). For these reasons, AOD data, the mass concentration of sulfate, and aerosol optical properties (absorption/-scattering coefficients) were used for CCN estimation in this study. Table 1 summarizes the description of the data used, and the details of each dataset are presented in Section 3.

Linear and multiple regression analyses were used to estimate the CCN concentrations. Statistical program for PASW 18.0 (SPSS Inc., Chicago, IL, USA) for Windows was used to determine the models. Since the Zeppelin station is located in an area with distinct seasonality of CCN concentration, each regression model was presented using data for the entire period from April 2007 to March 2013 and each season simultaneously to evaluate the models by season. The temporal resolutions of input data to the regression models are daily averages; however, they were multi-year monthly averages from January to December or monthly averages during the entire period for the linear regression model of CCN-AOD, since they showed large variations with high time resolution data in the CCN-AOD relationship.

3. Data

3.1. CCN

CCN concentration data (Jung et al., 2018) obtained from ground-based observations at the Zeppelin station were used. A commercially available Droplet Measurement Technologies CCN counter with one column (CCNC-100), managed by the Korea Polar Research Institute from 2007, was used to measure supersaturation (SS) at 0.2%, 0.4%, 0.6%, 0.8%, and 1% at a time resolution of 5 min scanning intervals (10 min for SS of 0.2%). After the 1% SS measurement, the cycle was restarted with 0.2% SS. In the CCN counter measurement system, the temperature of the CCN column increased in the streamwise direction. Supersaturation is determined by the streamwise temperature gradient, total flow rate, and pressure (Lance et al., 2006). In this study, the daily averaged CCN concentration at 0.4% SS using 5 min resolution data was employed. Monthly averaged data were calculated from daily averages. There is a high correlation between the number concentration of condensation nuclei (CN) and CCN at 0.4% supersaturation (Jayachandran et al., 2020; Nair et al., 2020). Therefore, the ratio of $CCN_{0.4}$/CN has been used in various studies as a CCN activation ratio (Andreae, 2009; Matsuki et al., 2010; Duan et al., 2017). In addition, this supersaturation level can represent convective clouds (Konwar et al., 2012), which have a substantial impact on climate. Andreae (2009) investigated the correlation between CCN at 0.4% SS and AOD at 500 nm; therefore, the results of this study using CCN concentrations at 0.4% SS for the Zeppelin station can be effectively compared with the global average result of Andreae (2009).

3.2. Aerosol optical properties from ground-based observations

AOD was measured under daylight conditions using a sun photometer, Type SP1a, located in Ny-Ålesund (78.923° N, 11.928° E), Svalbard. This photometer was manufactured by Dr. Schulz & Partner GmbH with ten wavelength intervals between $\lambda = 369$ and 1023 nm, a field of view of $1° \times 1°$, and a time resolution of 1 min (Graßl and Ritter, 2019). In this study, we used 1-min averaged AOD near $\lambda = 500$ nm from April 2007 to March 2013, and the AEs were calculated with AOD near 500 and 860 nm. To conduct the CCN-AOD linear regression analysis in Section 4.1.2, daily averaged AOD was calculated from the 1-min data, and monthly averages were then derived. The measurement principle

Table 1
Characteristics of CCN, AOD from ground-based measurements, MODIS, and MERRA-2 data.

Characteristics	CCN	AOD from ground-based measurements	MODIS	MERRA-2	Aerosol absorption coefficient	Aerosol scattering coefficient	Aerosol chemical composition
Dataset	CCN particle counter	Measured AOD by sun photometer, Type SP1a	• MOD08_D3 (Collection 6)	• MERRA-2 inst3_3d_gas_Nv	Modified Particle Soot Absorption Photometer (PSAP)	Integrating Nephelometer (TSI Inc., Model 3563)	Aerosols using a three-stage filter pack sampler
Temporal resolution	• 5-min average data	• One minute average data	• Three-hour average data	• Daily average data	• Hourly average data	• Hourly average data	• Daily average data
Location	Zeppelin station (11.89° E, 78.91° N)	Ny-Ålesund (11.928° E, 78.923° N)	11. 5° E, 78.5° N (Spatial resolution: 1° × 1°)	11.875° E, 79° N (Spatial resolution: 0.5° × 0.652°)	Zeppelin station (11.89° E, 78.91° N)	Zeppelin station (11.89° E, 78.91° N)	Zeppelin station (11.89° E, 78.91° N)
Number of data (Monthly and daily average)	• 55/72 • 1,535/2,192	• 43/72 • 518/2,192	• 42/72 • 641/2,192	• 72/72 • 2,192/2,192	• 1,688/2,192 (daily avg.)	• 919/2,192 (daily avg.)	• SO_4^{2-}: 1,713/2,192 • NaCl: 1,474/2,192 (daily avg.)
Wavelength		501 nm	550 nm	550 nm	525 nm	550 nm	
Supersaturation	0.4%						

and requisite corrections for obtaining the AOD were further described by Graßl (2019).

A modified Particle Soot Absorption Photometer (PSAP; Radiance Research, Inc., Seattle, WA, USA; Bond et al., 1999) was used to collect absorption coefficient (b_{abs}) data for the wavelength of 525 nm. This instrument produces a semi-continuous measurement of absorption by monitoring the change in transmittance across a filter using a 525 nm green light source. This instrument measures light absorption acquired from filter-based samples by theoretically applying Beer's law (Springston, 2018). BC dominates aerosol light absorption in the shortwave in the atmosphere emitted from anthropogenic and natural combustion sources or light-absorbing organic carbon, commonly referred to as brown carbon, which has not been revealed much for its absorption effect (Moosmüller et al., 2009). In this study, b_{abs} in the visible range was considered, and it was assumed that the effect of non-BC light--absorbing components was negligible (Liu et al., 2015; Chow et al., 2018; Zhang et al., 2020). Stohl et al. (2006) provided a more detailed description of absorption coefficient measurements. The PSAP for the Mt. Zeppelin Observatory has been in operation since 2002 (Schmeisser et al., 2018). In this study, we used the daily averaged data calculated using 1-h resolution data obtained from April 2007 to March 2013.

Scattering coefficients (b_{sca}) were measured using an integrating nephelometer (TSI Inc., Model 3563) operated at wavelengths of 450, 550, and 700 nm (Anderson et al., 1998) under almost dry conditions (RH $<$ 20% inside the instrument) at Mt. Zeppelin Observatory from January 2010 to March 2013 (Rastak et al., 2014). The daily averaged scattering coefficients at 550 nm calculated using 1-h resolution data were used in this study.

Filter samples used to analyze the chemical composition of aerosols were gathered daily at the Zeppelin station. The sampling was performed using a three-stage filter pack sampler, where the filters were exposed to air without any particle size separator, such as a cyclone or impactor. For protection against precipitation, the exposed filter substrate faces downward within the housing. Filters were analyzed by ion chromatography (Dionex, model ICS-2000; Aas et al., 2020). Among aerosol chemical components, sulfate (SO_4^{2-}) and sea salt (NaCl) were used in this study. Detection limits of 0.01 and 0.02 μg m^{-3} for sulfate and sea salt, respectively, were applied; thus, data below these values were removed. All aerosol filter sampled data are openly available at http://ebas.nilu.no.

3.3. MODIS

The Moderate Resolution Imaging Spectroradiometer (MODIS), operated by the National Aeronautical Space Administration (NASA), measures radiance at the top of the atmosphere (TOA) at 36 wavelengths from 0.41 to 14 μm with a viewing swath of 2330 km, providing near-global coverage each day (Salomonson et al., 1989; Ma et al., 2013). There are two polar orbit satellites with MODIS sensors as part of the NASA project. One is Terra, which has produced data since February 2000, and the other is Aqua, active since July 2002 (King et al., 2003). In this study, the daily averaged level 3 product from MODIS-Terra Collection 6 (MOD08) (Hubanks et al., 2015) with 1° × 1° spatial resolution was used for AOD at 550 nm wavelength under daylight conditions. All AOD data were selected in the nearest grid to the Zeppelin station, 78.5° N, 11.5° E. Monthly averages of AOD from MODIS were calculated from the daily data. The level 2 product from MODIS-Terra collection 6 (MOD04) with a 10 km × 10 km spatial resolution was also used for AE (calculated 550–860 nm AOD). Since level 2 MODIS AE product does not provide daily or monthly mean data, they were averaged in this study. All AE data were chosen within a 1° radius of the Zeppelin station considering MODIS AOD data used in this study have a 1° × 1° spatial resolution and referred to Wang et al. (2017). They were used on a daily or monthly average. Terra's orbit around the Earth is timed such that it passes from north to south across the equator in the morning, whereas Aqua passes from south to north over the equator in the afternoon. The AOD values over land varied within the expected uncertainty range of the MODIS retrieval (Glantz and Tesche, 2012). A detailed description of the MODIS aerosol algorithm can be found in Remer et al. (2005).

3.4. MERRA-2

The Global Modeling and Assimilation Office at NASA produced a second version of the MERRA reanalysis data, MERRA-2, which spans the entire modern era of satellites (i.e., 1980 to the present). In this study, we used the 3-hourly MERRA-2 AOD (M2IUNXGAS version 5.12.4) and AE data at 550 and 470–870 nm, respectively. Monthly averages of AOD from MERRA-2 were calculated from the daily data. We acquired the mass concentration of each chemical component from the hourly MERRA-2 aerosol diagnostics data (M2TUNXAER version 5.12.4). These MERRA-2 aerosol diagnostics data were calculated daily averaged for the multiple regression analysis in Section 4.2.3. These data have a spatial resolution of 0.5° × 0.625°, and all AOD and chemical component data were selected at 79.0° N, 11.9° E, which is the nearest grid to the Zeppelin station. These reanalysis data are obtained through the assimilation of aerosol modeling and observation, producing information for five species of aerosols (dust, sea salt, sulfate (SO_4^{2-}), BC, and organic carbon) through the coupling of the Goddard Chemistry Aerosol Radiation and Transport (GOCART) model and MERRA-2 reanalysis radiation data (Chin et al., 2002), from which AOD was obtained. MERRA-2 was used concurrently with aerosol and meteorological assimilations, and AOD measurements were taken from various National Oceanic and Atmospheric Administration Polar Operational Environmental Satellites, NASA Earth Observing System platforms, and NASA ground-based observations, including AERONET, MODIS, and the Advanced Very High-Resolution Radiometer (Buchard et al., 2017; Randles et al., 2017; Penna et al., 2018).

4. Results

4.1. Relationship between CCN and remote sensing data

4.1.1. Variation of CCN and AOD observation

Fig. 2 shows the time series of monthly mean values of AOD at 500 nm from ground-based measurements, AOD at 550 nm for MODIS and MERRA-2, CCN measurements at SS = 0.4%, and associated standard deviation calculated from daily averages at Zeppelin station during 2007–2013. The CCN concentrations in this study were comparable with previously reported data from remote continental regions (Andreae, 2009). The CCN number concentration ranged from 21 to 217 cm^{-3} with a minimum in October 2012, and a maximum in March 2010, and the AOD from ground-based measurements ranged from 0.02 to 0.13 with a minimum in October 2012 and a maximum in April 2009. AOD data from ground-based measurements are available only from March through September using a sun photometer since solar radiation is a prerequisite. Frequently observed AODs of over 0.12 are comparable with those typically measured at mid-latitude stations of northern continental areas. Both CCN and AOD showed similar seasonal variations during the analysis period. Generally, CCN increased during the winter and reached maxima in early spring, while it decreased during summer toward minima in autumn. AOD followed a similar pattern, increasing toward the late spring and decreasing during the summer. The CCN concentration showed higher variability than the AODs, as indicated in Fig. 2. The MERRA-2 AOD data had a comparatively low standard deviation and showed the least variability; whereas MODIS AOD data demonstrated a relatively higher standard deviation than the others, likely because there are relatively fewer data from MODIS passing over the Zeppelin station as the Terra is a polar-orbiting satellite. Therefore, interpretating quantitative comparisons of MODIS AOD directly with other measurement data must be done carefully.

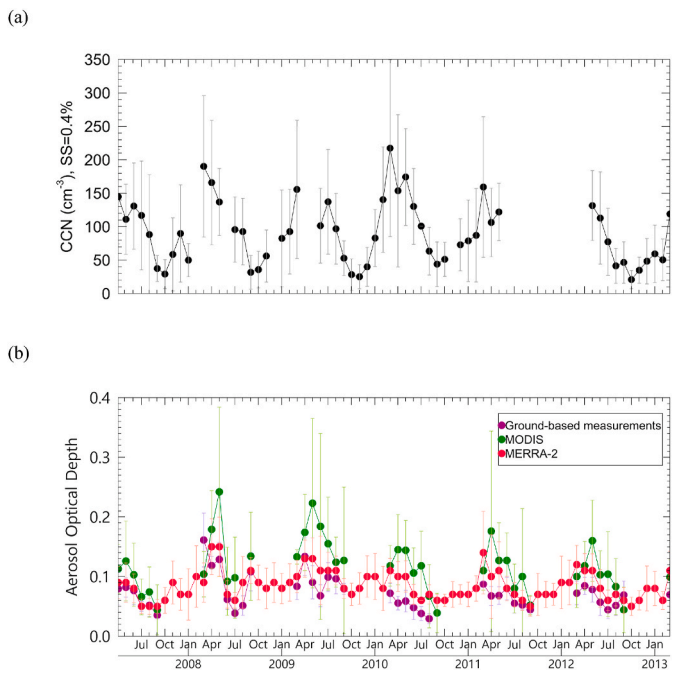

Fig. 2. Monthly variations of (a) CCN at SS = 0.4%, (b) AOD from ground-based measurements at 500 nm, MODIS AOD at 550 nm, and MERRA-2 AOD at 550 nm, from April 2007 to March 2013 at Zeppelin and Ny Ålesund observatories. Error bars indicate the standard deviation of the daily averaged data.

Fig. 3 shows the multi-year monthly means of CCN concentration and AOD during 2007–2013. As shown in Fig. 2, both CCN and AOD exhibit similar seasonal trends, indicating that AOD and CCN are closely related, as revealed in previous studies (Andreae, 2009; Romakkaniemi et al., 2012; Tang et al., 2014). CCN contributes to AOD, even though AOD represents not only the atmospheric boundary layer but also the vertically integrated attenuation. The CCN concentration exhibited pronounced seasonal variation. The concentration peaks in March with declining values during summer, showing a minimum in October. Meanwhile, AOD from ground-based measurements was also high in spring and low in summer to early fall; however, the variation was smaller than that of the CCN concentration. The MERRA-2 AOD followed the same seasonal trend as AOD from ground-based measurements and in-situ CCN measurements. As mentioned above, MODIS AOD was biased with others due to issues with time synchronization. Still, the maximum AOD appeared in the spring, similar to ground-based and MERRA-2 AOD measurements. AOD from ground-based measurements and MODIS AOD were compared with MERRA-2 AOD, showing R^2 values of 0.62 and 0.60 with statistical significance levels ($p < 0.01$), respectively (Fig. 4(a) and b). These results suggest that MERRA-2 AOD data can serve as a good proxy in the Arctic region where ground-based AOD observations or MODIS AOD data are not available.

4.1.2. Relationship between CCN and AOD observations

Table 2 shows the seasonal mean values with corresponding standard deviations for CCN number concentration, ground-based AOD observations, and remote-sensing-derived AOD from MODIS and MERRA-2 for 2007–2013. The seasonality of the ground-based AOD observations is similar to that of MERRA-2, which assimilates various observational data, showing high AOD in spring. The high seasonality of CCN concentrations in the Arctic is driven by a sizeable anthropogenic influence in winter and spring when sources from Russia and Kazakhstan (winter) and East Asia (spring) are the most important (Fisher et al., 2011).

Fig. 5 shows the multi-year seasonal mean of the ground-based AOD–CCN relationship based on the daily averaged data. For the

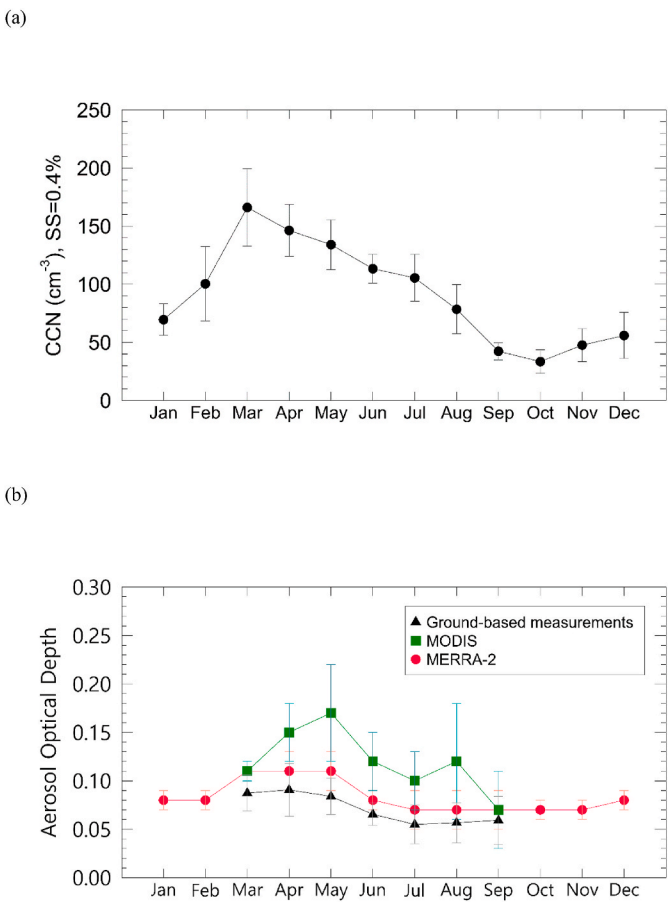

Fig. 3. Multi-year monthly mean variations of (a) CCN and (b) AOD from ground-based measurements, MODIS, and MERRA-2, during the analysis period 2007–2013. For the variations, CCN is obtained at SS = 0.4%, AOD from ground-based measurements at WL = 500 nm, and, for MODIS and MERRA-2, AOD at 550 nm. Error bars indicate the standard deviation of the daily averaged values.

entire period, the average CCN number concentration was 109 cm^{-3} (standard deviation: 47 cm^{-3}), and AOD from ground-based measurements was 0.068 (standard deviation: 0.026). Among the three seasons, aerosol in spring had the highest AOD and CCN through the impact of Arctic haze. Nevertheless, aerosols were classified as remote in all seasons in this study, according to the suggested method by Andreae (2009). This is because the method by Andreae (2009) was carried out on a global scale. By contrast, low aerosol concentrations present in the Arctic, even though they are influenced by long-range transport from mid-latitude air masses. Thus, AOD and CCN in this study are below the threshold for being classified as polluted. There is a limitation in the direct comparison of Andreae (2009) from various studies, various regions, and different periods with presented results in this research from continuous observational data at the Zeppelin station. However, the seasonal averaged CCNs and AODs in this study are in good agreement with the relation from Andreae (2009), except in autumn. This study shows a low CCN level in autumn compared with the global average at a given AOD.

Fig. 6 shows a scatterplot of the multi-year monthly averaged CCN and AOD at the Zeppelin station from their daily averages. The linear regression results showed high adjusted R^2 values of 0.59 for CCN–AOD from ground-based measurements (Fig. 6(a)) and 0.66 for CCN-MERRA-2 AOD (Fig. 6(b)), with statistical significance at the $p < 0.05$, and $p < 0.01$ levels. The ratio of AOD to CCN was higher in spring than in the other seasons, which is in accordance with Jung et al. (2018), demonstrating higher ratios of CCN to $CN_{>10\ nm}$ in spring when Arctic haze is

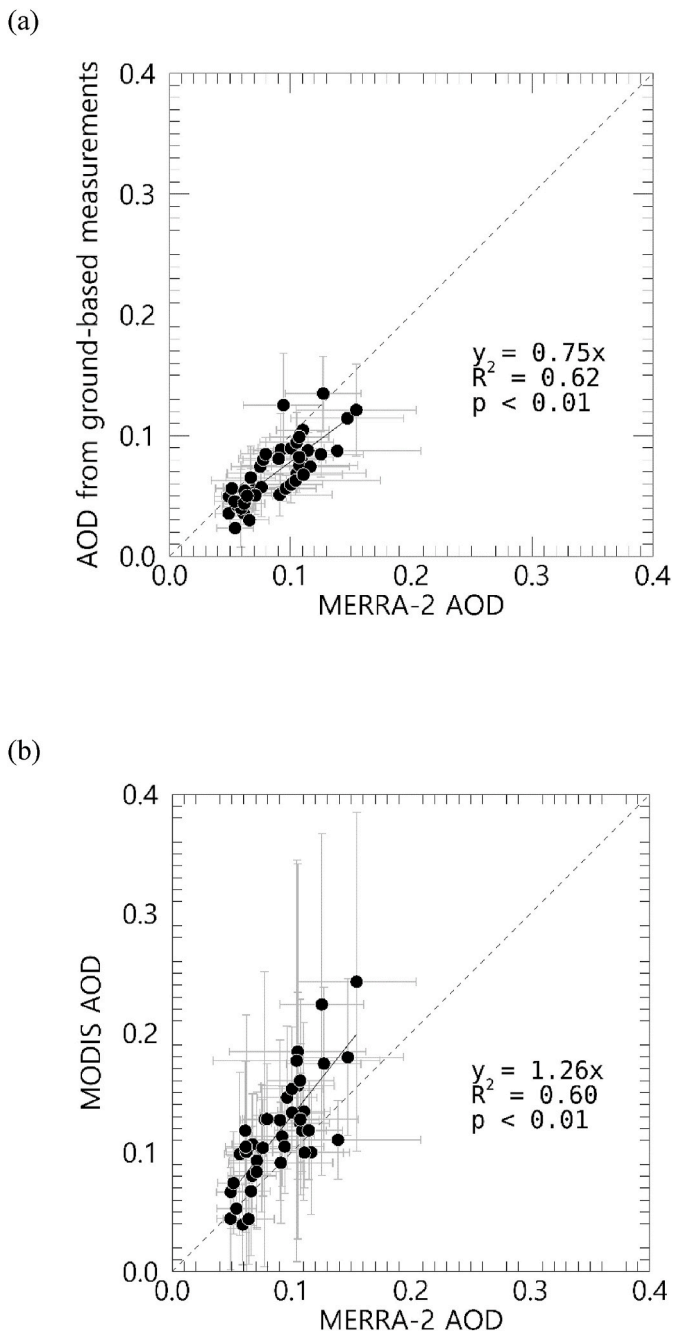

Fig. 4. Comparisons of monthly averaged MERRA-2 AOD with monthly averaged (a) AOD from ground-based measurements and (b) MODIS AOD from daily averaged AOD. The standard least-squares regressions (thick solid lines) yield (a) $AOD_{measurement} = 0.74\ AOD_{MERRA\text{-}2}$, $R^2 = 0.53$, $p < 0.01$ and (b) $AOD_{MODIS} = 1.26\ AOD_{MERRA\text{-}2} + 0.01$, $R^2 = 0.52$, $p < 0.01$, respectively. Error bars indicate the standard deviation of the daily averaged AOD. The gray dashed lines represent the ideal 1 : 1 case.

dominant at Zeppelin station. Monthly averaged CCNs and AODs from ground-based measurements are presented (Fig. 6(c)), which show that both CCN and AOD data have large monthly variations. As shown in Fig. 6(c), the relation becomes consistent by excluding outliers, but the slope becomes lower than the multi-year monthly averaged data. Arctic CCN and AOD are influenced by aerosol chemical composition, which has strong seasonality. To determine the CCN–AOD relationship, multiple regression models using aerosol chemical composition variables were suggested in Section 4.2 for various seasons.

Table 2
Seasonally averaged CCN concentrations and AOD for the period April 2007 to March 2013 (mean ± standard deviation).

Season	CCN [cm^{-3}] (SS = 0.4%)	AOD from ground-based measurements (500 nm)	MODIS AOD (550 nm)	MERRA-2 AOD (550 nm)
Spring	130 ± 89	0.087 ± 0.022	0.125 ± 0.090	0.106 ± 0.043
Summer	85 ± 65	0.059 ± 0.018	0.087 ± 0.156	0.067 ± 0.031
Autumn	33 ± 32	0.054 ± 0.026	0.052 ± 0.077	0.064 ± 0.027
Winter	58 ± 66	–	–	0.074 ± 0.035

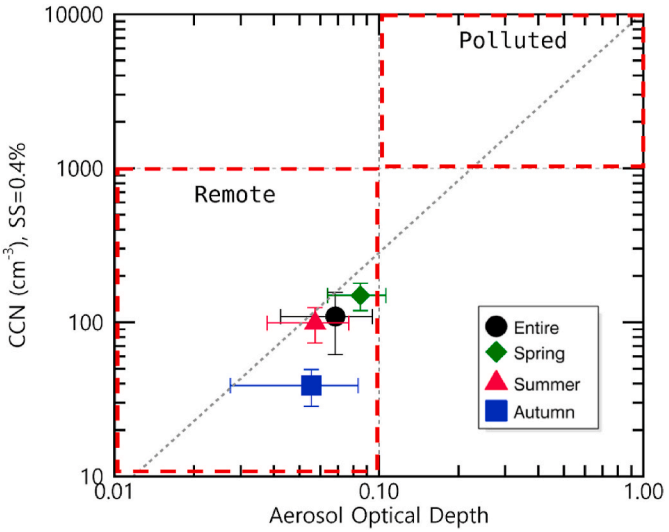

Fig. 5. Comparisons of CCN with AOD from ground-based measurements composited by season. Error bars indicate the standard deviation of the daily averaged CCN or AOD. All data are classified as remote continental marine aerosols (Andreae, 2009). The dashed line indicates a regression, AOD at 500 nm = $0.0027 \cdot [CCN0.4]^{0.640}$, from Andreae (2009) for reference.

4.1.3. Relationship between CCN and Ångström exponent

The physicochemical characteristics of the aerosols can explain the seasonal differences in the properties of AOD and CCN. Chemical composition and particle size distribution are important aerosol characteristics determining their optical properties in the Arctic region (Lund et al., 2004; Jung et al., 2018). Jung et al. (2018) compared the parameterized aerosol number size distribution at the Zeppelin station in spring with that in summer. These distributions were based on ground station measurement data from 2007 to 2013. The log-normal size distributions of the Aitken and accumulation modes were defined by three parameters (geometric mean diameter, geometric standard deviation, and total number concentration). In that study, there was a distinct increase in the accumulation mode in spring, and the Aitken mode became more pronounced in summer (Tunved et al., 2013; Jung et al., 2018), suggesting that the increase in the Aitken mode particles during summer is linked to more frequent particle formation. Low aerosol concentrations during autumn were also indicated for both the Aitken and accumulation modes.

AE is a conventional parameter that characterizes the aerosol size distribution based on aerosol optical properties. It is a part of the equation that describes the dependence of AOD or aerosol extinction coefficient on wavelength and is inversely related to the average aerosol particle size. Hence, AE increases as the particle size decreases. Fig. 7(a) and (b) show the monthly and seasonal composite variations, respectively, of AE from ground-based measurements, MODIS, and MERRA-2

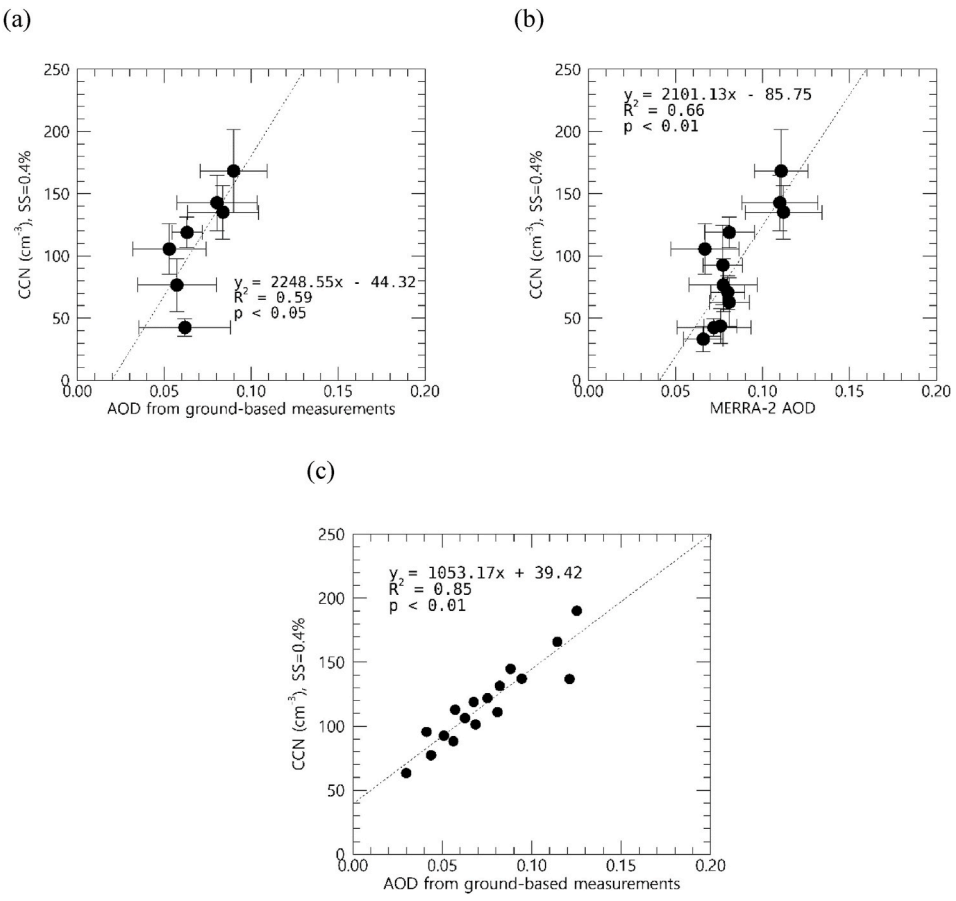

Fig. 6. (a) Comparisons of multi-year monthly averaged CCN with multi-year monthly averaged AOD from ground-based measurements and (b) MERRA-2 AOD. The standard least-squares regressions (thick solid lines) yield (a) $CCN_{0.4}$ = 1906.80 AOD – 23.21, $R^2 = 0.72$, $p < 0.05$ and (b) $CCN_{0.4}$ = 1980 AOD – 76.34, $R^2 = 0.68$, $p < 0.01$, respectively. Error bars indicate the standard deviation of the daily averaged CCN or AOD. (c) Comparisons of monthly averaged CCN with monthly averaged AOD from ground-based measurements with 95% confidence limits.

data. The AE shows low values in early spring and high levels in late spring and early summer, decreasing again in winter, based on the MERRA-2 and MODIS AE data. However, AE from ground-based measurements shows less monthly or seasonal variation than MERRA-2 or MODIS AE. The seasonal variations of AE are in agreement with those from previous studies that show that in spring, accumulation mode aerosols are dominant, whereas, in summer, Aitken and nuclei mode size aerosols dominate the aerosol size distribution (Ström et al., 2003; Tunved et al., 2013; Jung et al., 2018).

Rodríguez et al. (2012) and Chen et al. (2016) classified aerosols into four types based on AOD and AE (α). The aerosol categories were continental (AOD <0.16 and α > 1.1), maritime (AOD <0.16 and α < 1.1), smoke/pollution (AOD ≥0.16 and α ≥ 1.1), and mixture of dust and pollution (AOD ≥0.16 and α < 1.1). Based on this classification, all ground-based aerosol measurements have been interpreted as continental aerosol type (Fig. 8), which refers to relatively small particles with low AOD that are transported from a remote area. According to the Freud et al. (2017) experiment, which involved a back-trajectory model, Zeppelin contains source regions for smaller particles in the accumulation mode (e.g., Mahowald et al., 2014), effective for light scattering and absorption, in western Russia and western Kazakhstan. They are located below 50° N latitude and represent global hot spots for desert dust (Engelstaedter and Washington, 2007). However, AEs from MERRA-2 are classified as maritime aerosols only in spring (Fig. 8). This may be related to underestimating the MERRA-2 AE in most global regions, including Europe (Gueymard et al., 2019).

4.2. CCN derived from in-situ observations and reanalysis data

4.2.1. CCN derived from chemical species observations

The ability of aerosol particles to act as CCN at a given supersaturation is related to the chemical composition, particle size, and mixing state. In particular, sulfate species in Arctic aerosols are particularly efficient CCN (Gutman and Reissell, 2011). Menon et al. (2002) diagnosed the number concentration of CCN ([CCN]) as a function of the mass concentration of SO_4^{2-} (sulfate) aerosols, with a correlation coefficient of 0.69, from the observed data at Mount Gibbes site, North Carolina, in the southeastern United States during summer 1995.

$$logCCN = (0.62 \pm 0.19) log\left[SO_4^{2-}\right] + (2.2 \pm 0.17) \quad (1)$$

Giardi et al. (2016) found that SO_4^{2-} was the dominant mass among the sampled soluble particles from sub-micrometer aerosols at the Gruvebadet Observatory, located at approximately 50 m asl, 800 m southwest of the Ny-Ålesund village (78.923° N, 11.928° E), Svalbard Islands, from March to September 2013. Moreover, $nss - SO_4^{2-}$ was the most abundant species, followed by sea salt, compared to other ionic aerosol components, such as Na^+, Cl^-, and NH_4, with measurements using a cut-off size of 20 μm during the campaigns from February to May 2001 at the Zeppelin site (Teinilä et al., 2004). Based on these studies, to apply the model of Eq. (1) to the Zeppelin station, the following regression model was suggested for the analysis period in this study, based on the measurement data of CCN concentrations and sulfate mass concentrations with the data indicated in Section 3. Data (Aas et al., 2020).

$$\log_{10}[\mathrm{CCN}] = a_1 \cdot \log_{10}\left[SO_4^{2-}\right] + c \quad (2)$$

where CCN and SO_4^{2-} are in units of cm^{-3} and $\mu g \cdot m^{-3}$, respectively. Table 3 shows the multiple regression coefficients, and correlation coefficients derived from the daily averaged CCN number concentration ([CCN]) and the mass concentration of sulfate. The correlation coefficient (R) ranged from 0.425 to 0.745 from summer to winter. All

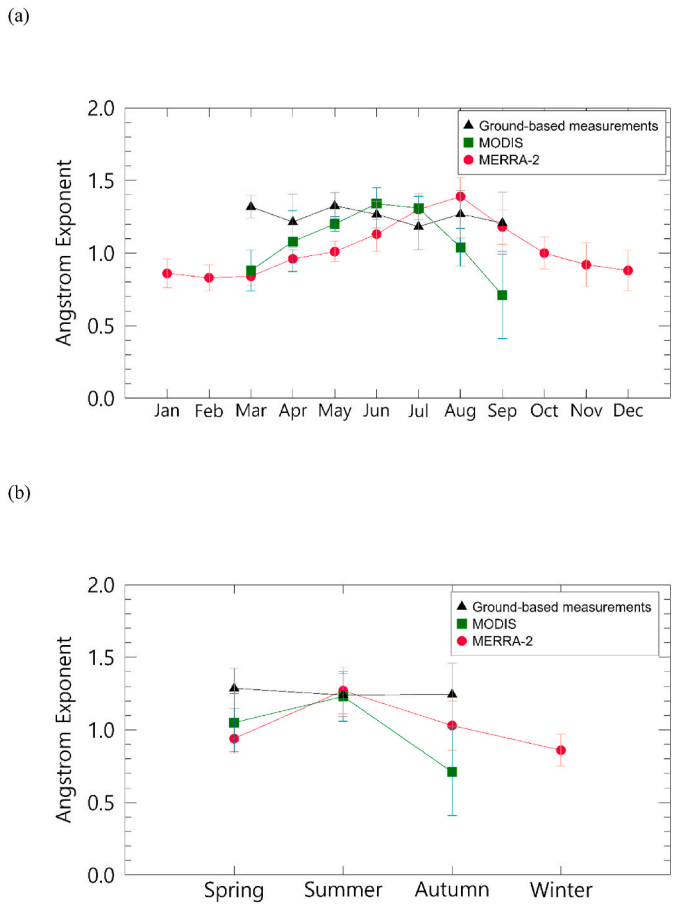

Fig. 7. (a) Monthly and (b) seasonal, variation of the AE obtained from ground-based AOD measurements, MODIS, and MERRA-2. Error bars indicate the standard deviation of the daily averaged AE.

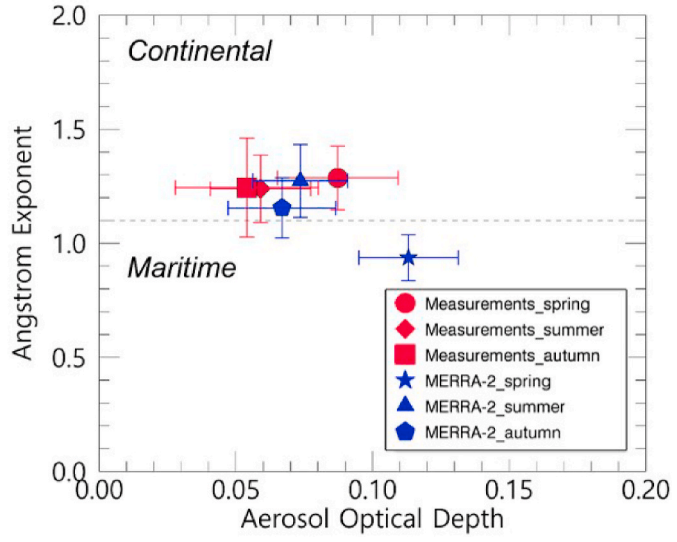

Fig. 8. Comparisons of the calculated AE with AOD from ground-based measurements and MERRA-2. Error bars indicate the standard deviation of the daily averaged AE or AOD.

regression coefficients were positive, indicating that SO_4^{2-} may contribute to CCN. The entire dataset exhibited a regression coefficient of 0.647 for sulfate, comparable to that of Menon et al. (2002). The regression coefficient for sulfate in autumn and winter was relatively high; however, it was low in spring and summer. This may be because of the chemical contribution from other types of aerosols related to CCN. For example, long-range transport frequently occurs in spring, which results in the accumulation of BC, and the formation of secondary organic aerosols is common with strong irradiance in summer near the Arctic region. Since sea salt is also a dominant component along with sulfate at the Zeppelin station (Teinilä et al., 2004), a CCN estimation regression was examined using sea salt as an independent variable with sulfate. The result was not statistically significant ($p > 0.05$ for the entire period; refer to Table. S1). One reason for this may be, based on the measurements at Zeppelin station during a field campaign during the spring season in 2001 (Teinilä et al., 2004), most sea salt particles exist in the coarse mode size, which contributes only a small fraction of CCN activation (Andreae and Rosenfeld, 2008). In addition, sea salt may not contribute to CCN formation efficiently during spring and summer due to relatively low wind speeds (Hudson et al., 2011; Cisek et al., 2017).

Table 3
Coefficients relating log10 aerosol chemical composition to log10 CCN (as in Eq. (2)) for each species based on daily averaged data by season for the period April 2007 to March 2013. N reflects the number of data points used to retrieve each coefficient. All coefficients are statistically significant ($p < 0.05$).

Coefficients	Spring	Summer	Autumn	Winter	All
Constant	2.456	2.343	2.278	2.510	2.468
a_1 (SO_4^{2-})	0.483	0.390	0.612	0.778	0.649
r	0.618	0.425	0.523	0.745	0.647
N	347	307	264	282	1,200

The CCN concentration, estimated using Eq. (2), was compared with the observed CCN from Jung et al. (2018), as shown in Fig. 9(a). The CCN concentrations derived from Eq. (2) and Menon et al. (2002) showed smaller estimates compared with in situ observational data. However, the correlation coefficient was higher in this study (0.73) than in Menon et al. (2002) (0.62), and the slope in this study was closer to 1 than that reported by Menon et al. (2002). The reproduced CCN concentrations in this model were shown to be in better agreement with the in situ CCN observation data in Ny-Ålesund than the reproduced CCN from Menon et al. (2002). Ratios of CCN to CN (particle concentration; diameter >10 nm; Jung et al., 2018) are also presented in Fig. 9(b) and (c), using the estimated CCN from Eq. (2), and the observed CCN from Jung et al. (2018). The averages for each season in Fig. 9(b) were comparable to those from Fig. 9(c), and the seasonal trend was similar to the observed trend but with ratios of high standard deviation for each season.

4.2.2. *CCN derived from scattering and absorption coefficients*

As shown in the CCN–AOD relationship, in Section 4.1.2, the CCN concentration can be expressed by aerosol light scattering and light absorption, represented by the aerosol scattering coefficient (b_{sca}) and absorption coefficient (b_{abs}), respectively, with in-situ measurements (see Section 3.2). The aerosol absorption coefficient (b_{abs}) is strongly related to light-absorbing aerosols such as BC or BC containing aerosols. Meanwhile, other aerosol components, such as dust, sea salt, sulfate, and organic carbon, contribute mainly to light-scattering, although sulfates make up the primary effect (see Table S2 in)Eq. (S1). Based on this, we propose a regression model for CCN with b_{sca} and b_{abs}terms as follows:

$$\log_{10}[CCN] = a_1 \cdot \log_{10}[b_{sca}] + a_2 \cdot \log_{10}[b_{abs}] + c \quad (3)$$

where b_{sca} and b_{abs} are expressed in units of Mm^{-1}. Table 4 shows the parameter values for the regression model in Eq. (3) derived from the daily averaged CCN, b_{sca} and b_{abs}. This model estimates the CCN with high correlation coefficients for all seasons. The correlation coefficients ranged from 0.623 to 0.954 in autumn and winter, at satisfactory significance levels. In most of the seasons and for the entire data, b_{sca} is more significant than b_{abs}, with higher coefficients showing results comparable to those of previous studies (McCoy et al., 2017). However,

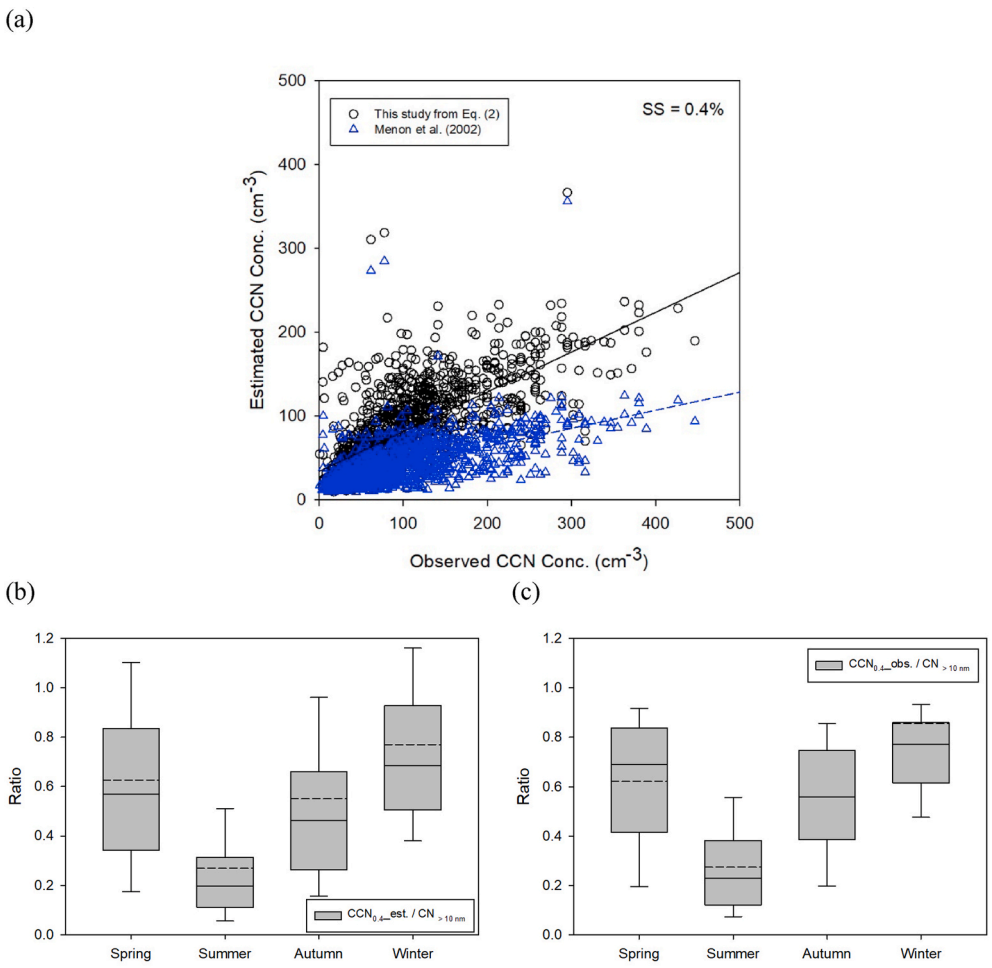

Fig. 9. (a) Estimated daily averaged CCN concentration by Eq. (2) (black) and by Menon et al. (2002) (blue) and observed daily averaged CCN concentration from Jung et al. (2018). The standard least-squares regressions (black solid and blue dashed line) yield $CCN_{estimated} = 0.47\ CCN_{observed} + 34.05$, $R^2 = 0.53$ ($p < 0.01$) for this study and $CCN_{estimated} = 0.22\ CCN_{observed} + 20.71$, $R^2 = 0.38$ ($p < 0.01$) for Menon et al. (2002), respectively. (b) Box plots of the ratio of estimated CCN concentration from Eq. (2) to CN from Jung et al. (2018). The mean (dashed line), median (solid line), 25th and 75th percentiles (lower and upper box), and 10th and 90th percentiles (lower and upper whiskers) are shown for each box. (c) Same as (b) except for observed CCN from Jung et al. (2018). (For interpretation of the references to colour in this figure legend, the reader is referred to the Web version of this article.)

Table 4
Coefficients relating log10 absorption and scattering coefficients to log10 CCN (as in Eq. (3)) for each species, based on daily averaged data by season. N reflects the number of data used to retrieve each coefficient. All coefficients are statistically significant ($p < 0.05$).

Coefficients	Spring	Summer	Autumn	Winter	All
Constant	2.109	2.164	1.709	1.706	1.899
a1 (b_sca 550 nm)	0.242	0.414	0.301	0.559	0.357
a2 (b_abs 525 nm)	0.330	0.246	0.203	0.414	0.236
r	0.640	0.702	0.623	0.954	0.692
N	119	101	133	141	494

this is reversed in spring, which means that the role of BC, represented as the absorption coefficient, may be more critical to the CCN concentration than the other aggregated light non-absorbing aerosol chemical components, which represent the scattering coefficient.

It is well known that the Arctic environment can accumulate aerosols through the transport of pollution from the continental northern mid-latitudes, known as Arctic haze (Jacob et al., 2010). BC concentrations have been observed to increase significantly in winter and spring, similar to sulfate and CCN concentrations at Alert (82.5° N, 62.5° W) (Sharma et al., 2004; Gong et al., 2010) and Zeppelin station (Hopper et al., 1994; Eleftheriadis et al., 2009). It is well known that BC particles are hydrophobic and do not act as effective CCN, but when internally mixed with hydrophilic materials, they can act as CCN (Kristjánsson, 2002). However, the quantitative relationship between the coating on the BC particles and their hygroscopic properties is unknown, and timescale studies on the transition from hydrophobic to hydrophilic have also been conducted (McMeeking et al., 2011; Liu et al., 2013; Zhang et al., 2015; Perring et al., 2017; Li et al., 2018). During the Arctic spring and winter, the boundary layer is stable and stratified because of low atmospheric temperature and sparse sunlight, and long-range transport of air pollutants arriving in the Arctic dominates. In addition, aerosol scavenging is minimized owing to minimal cloud formation. Therefore, air pollutants remain in the boundary layer for an extended period. Accordingly, aerosols are aged, internally mixed, and the initially hydrophobic BC particles can efficiently act as CCN by coating and mixing with diverse hygroscopic materials (Sharma et al., 2004; Raatikainen et al., 2015).

The CCN estimated using Eq. (3) was compared with the observed CCN from Jung et al. (2018) in Fig. 10(a), with a good agreement (correlation coefficient: 0.08, $p < 0.01$). The estimated CCN tends to underestimate but shows better performance than that given by Eq. (2). As shown in Fig. 10(b) and (c), the CCN to CN ratio in this study varied widely for each season, and the average value was higher in spring and lowered in the other seasons than the observations. However, the overall yearly trend by season (decrease in summer and increase afterward) was consistent with the observations.

4.2.3. CCN derived from MERRA-2 AOD

According to Zhou et al. (2001), aged aerosols from long-range transport in the Arctic are believed to constitute the majority of the highly hygroscopic particles. In addition, previous studies have demonstrated that soluble aerosol species are incorporated into cloud droplets more often than BC (Hallberg et al., 1994). However, Bond et al. (2013) found that aging BC after emission could reduce the critical supersaturation of BC-containing particles, as the soluble mass increases

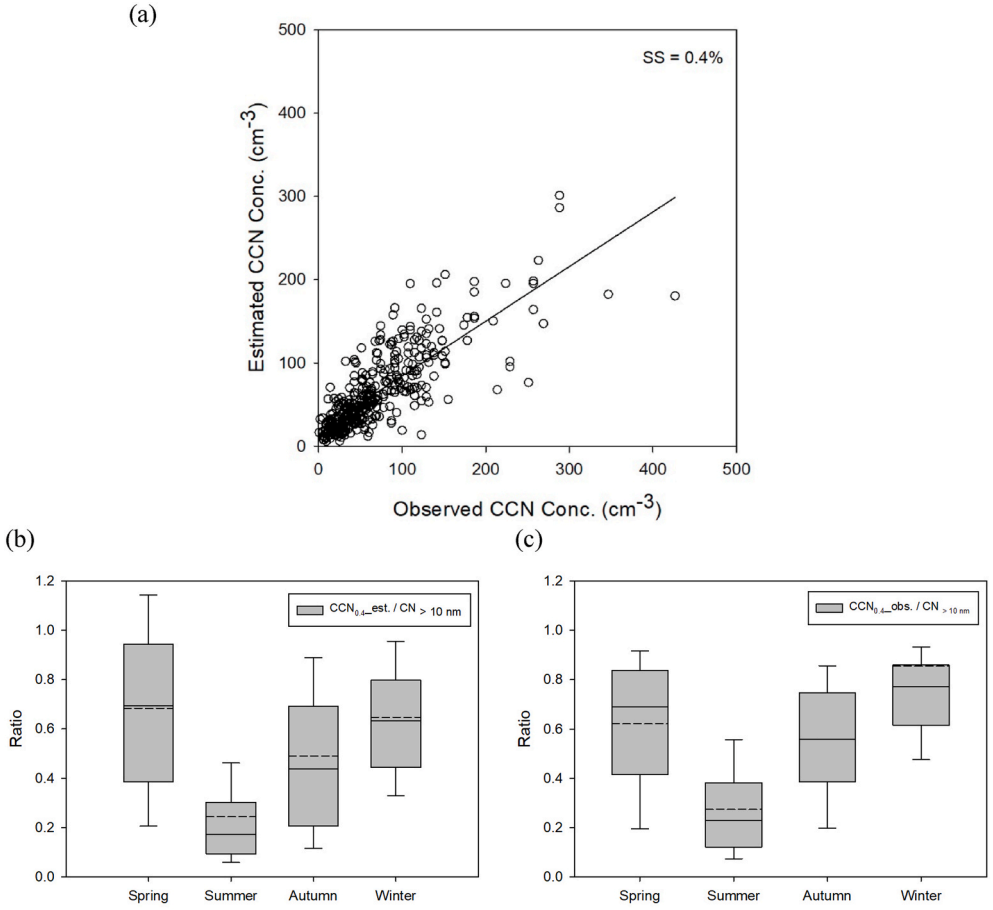

Fig. 10. (a) Estimated daily averaged CCN concentration from Eq. (3) and observed daily averaged CCN concentration from Jung et al. (2018). The standard least-squares regressions (solid lines) yields $CCN_{estimated} = 0.66\ CCN_{observed} + 18.95$, $R^2 = 0.64$ ($p < 0.01$). (b) Box plots of estimated CCN concentration from Eq. (3) to CN from Jung et al. (2018) ratio. The mean (dashed line), median (solid line), 25th and 75th percentiles (lower and upper box), and 10th and 90th percentiles (lower and upper whiskers) are shown for each box. (c) Same as (b) except for observed CCN from Jung et al. (2018).

both the particle volume and hygroscopicity. Furthermore, Maskey et al. (2017) found that BC coated with sulfuric acid, levolucosan, or succinic acid species (≈10% volume fraction) can be activated as CCN at a supersaturation of 0.5%. Consequently, for these reasons, the role of BC is a crucial factor in CCN activation near the Zeppelin station.

We also derived the relationship between the CCN number concentration and AOD from the MERRA-2 reanalysis data at the Zeppelin station. In the MERRA-2 reanalysis, two aerosol chemical compositions (SO_4^{2-} and BC) were considered to demonstrate the CCN–AOD relationship. The relationship between CCN and AOD resolved by chemical composition can be expressed as

$$\log_{10}[CCN] = a_1 \cdot \log_{10}[AOD_{SO4^{2-}}] + a_2 \cdot \log_{10}[AOD_{BC}] + c \quad (4)$$

where CCN from ground-based measurements are in units of cm^{-3} and $AOD_{SO4^{2-}}$, AOD_{BC} are AOD of sulfate and AOD of BC, respectively, from MERRA-2. Table 5 presents the multiple regression coefficients and correlation coefficients derived from the daily averaged CCN number concentration and $AOD_{SO4^{2-}}$, $AOD_{BC}$of MERRA-2. As presented in Table 5, all coefficients and their significance levels vary by season. The correlation coefficients from autumn to winter ranged from 0.113 to 0.331, with a correlation coefficient of 0.373 for the entire duration. The highest correlation coefficient was exhibited in winter, as shown in the results derived from the aerosol chemical concentration (Table 3) and absorption/scattering coefficient data (Table 4). Nevertheless, one possible reason for these overall low correlations is that BC may be overestimated by MERRA-2, especially in the free troposphere (Schwarz et al., 2013; Randles et al., 2017). Therefore, a model derived from AODs for aerosol chemical components of MERRA-2 should be used with caution because of the large uncertainties of the model.

Table 5
Coefficients relating log10 chemical composition resolved AOD from MERRA-2 to log10 CCN (as in Eq. (4)) for each species based on daily averaged data by season. N reflects the number of data used to retrieve each coefficient.

Coefficients	Spring	Summer	Autumn	Winter	All
Constant	2.668**	2.995**	2.827**	2.293**	4.572**
a1 (AOD_{SO4})	0.346**	0.276**	0.075	0.785**	0.363**
a2 (AOD_{BC})	0.039	0.273**	0.468*	−0.220	0.866**
r	0.226	0.227	0.113	0.331	0.373
N	378	419	396	342	1,535

*p < 0.1, **p < 0.05.

5. Conclusions

In this study, the CCN–AOD relationship was investigated based on the CCN data collected for the period 2007–2013 at the Zeppelin Observatory, Svalbard. For the AOD remote sensing data, ground-based measurements and MODIS data, as well as the MERRA-2 reanalysis, were used. The seasonal characteristics of AOD, as well as long-term trends, were also considered. Moreover, the CCN number concentration was related to the concentration of the aerosol chemical composition, absorption/scattering coefficient, or chemically resolved AOD obtained from the measurement and MERRA-2 reanalysis.

A high degree of correlation ($R^2 = 0.59$) for the multi-year CCN-AOD linear regression was determined with the observational data. The parameter AE, which is related to the size distribution, shows a high value during summer when relatively low AOD observed. This indicates the existence of small particles during summer. Hence, the small particles from active nucleation with high marine biota productivity can be assumed to promote sulfate formation, which contributes to CCN. Using the methods of Rodríguez et al. (2012) and Chen et al. (2016), all of the

ground-based aerosol measurements have been interpreted as continental aerosol types, affected by aerosols from low latitude areas.

In this study, three CCN derivation models were presented with a linear regression method, using the sulfate mass concentration measurement data from Menon et al. (2002), and two multi-linear regression methods using data from aerosol optical properties (i.e., aerosol absorption coefficients, scattering coefficients, and chemically resolved AOD). In the equation considering the sulfate mass concentration, the model presented in this study better correlated with the observed CCN than that of Menon et al. (2002). The model using aerosol absorption and scattering coefficients showed the most significant results among the three models presented. This explains the deep link between aerosol optical properties and CCN and the large contribution of light-absorbing aerosols such as BC to CCN. CCN concentration considerably depends on light-absorbing aerosols, demonstrating similar monthly variations with b_{abs} and BC concentrations. Notably, light-absorbing aerosols are important for CCN activation in the Arctic as well as sulfate, which was originally thought to be important. This is because although the Zeppelin station is in the Arctic, the location is exposed to long-range pollution transport, especially in winter and spring, during the Arctic haze. The stable and stratified boundary layer conditions in winter are efficient for transporting aerosols with hygroscopic materials in the air. We suggest that the model using aerosol absorption coefficients and scattering coefficients can estimate CCN to a certain degree. However, the CCN estimation derived from the AOD_{SO4} and AOD_{BC} of the MERRA-2 data should be used with caution because of the high uncertainty of the model.

Credit author statement

YJY, TJY, BYL: Conceptualization, **YPK, SHA:** Methodology, **SHA, CHJ, YJY :** Data curation, Writing- Original draft preparation. **CR, WA:** resources, Investigation. **SHA, CHJ, JYL :** formal analysis, **CR, WA, RK, JS, PT:** Validation.: **SHA, YJY, YPK, CHJ:** Writing- Reviewing and Editing.

Declaration of competing interest

The authors declare that they have no known competing financial interests or personal relationships that could have appeared to influence the work reported in this paper.

Acknowledgments

This research was supported by a National Research Foundation of Korea Grant from the Korean Government (MSIT) (NRF-2021M1A5A1065425/KOPRI-PN21011, and NRF-2021M1A5A1065672). The measurements of sulfate and sea salt in aerosols at Zeppelin Mountain were financed by the Norwegian Environment Agency. We would also like to thank the Swedish Environmental Protection Agency (Naturvårdsverket) for their long-term support of aerosol observations at the Zeppelin station. This work was also partly supported by the ACAS project funded by the Knut and Alice Wallenberg Foundation (KWA) and the funding agency FORMAS. The authors would also like to thank the Norwegian Polar Institute (NPI) for their long-lasting and substantial support of observations at the Zeppelin station used in this study.

Appendix A. Supplementary data

Supplementary data to this article can be found online at https://doi.org/10.1016/j.atmosenv.2021.118748.

References

Aas, W., Eckhardt, S., Fiebig, M., Solberg, S., Yttri, K.E., 2020. Monitoring of Long-Range Transported Air Pollutants in Norway. Annual Report 2019. NILU Rapport.

Anderson, T.L., Ogren, J.A., 1998. Determining aerosol radiative properties using the TSI 3563 integrating nephelometer. Aerosol. Sci. Technol. 29, 57–69.

Andreae, M., Rosenfeld, D., 2008. Aerosol–cloud–precipitation interactions. Part 1. The nature and sources of cloud-active aerosols. Earth Sci. Rev. 89, 13–41.

Andreae, M.O., 2009. Correlation between cloud condensation nuclei concentration and aerosol optical thickness in remote and polluted regions. Atmos. Chem. Phys. 9.

Bond, T.C., Anderson, T.L., Campbell, D., 1999. Calibration and intercomparison of filter-based measurements of visible light absorption by aerosols. Aerosol Sci. Technol. 30, 582–600.

Bond, T.C., Doherty, S.J., Fahey, D.W., Forster, P.M., Berntsen, T., DeAngelo, B.J., Flanner, M.G., Ghan, S., Kärcher, B., Koch, D., 2013. Bounding the role of black carbon in the climate system: a scientific assessment. J. Geophys. Res.: Atmospheres 118, 5380–5552.

Boucher, O., Lohmann, U., 1995. The sulfate-CCN-cloud albedo effect. Tellus B 47, 281–300.

Bréon, F.-M., Tanré, D., Generoso, S., 2002. Aerosol effect on cloud droplet size monitored from satellite. Science 295, 834–838.

Buchard, V., Randles, C., Da Silva, A., Darmenov, A., Colarco, P., Govindaraju, R., Ferrare, R., Hair, J., Beyersdorf, A., Ziemba, L., 2017. The MERRA-2 aerosol reanalysis, 1980 onward. Part II: evaluation and case studies. J. Clim. 30, 6851–6872.

Chen, Y.-C., Hamre, B., Frette, Ø., Muyimbwa, D., Blindheim, S., Stebel, K., Sobolewski, P., Toledano, C., Stamnes, J.J., 2016. Aerosol optical properties in northern Norway and Svalbard. Appl. Opt. 55, 660–672.

Chin, M., Ginoux, P., Kinne, S., Torres, O., Holben, B.N., Duncan, B.N., Martin, R.V., Logan, J.A., Higurashi, A., Nakajima, T., 2002. Tropospheric aerosol optical thickness from the GOCART model and comparisons with satellite and Sun photometer measurements. J. Atmos. Sci. 59, 461–483.

Chow, J.C., Watson, J.G., Green, M.C., Wang, X., Chen, L.-W.A., Trimble, D.L., Cropper, P.M., Kohl, S.D., Gronstal, S.B., 2018. Separation of brown carbon from black carbon for IMPROVE and Chemical Speciation Network PM2. 5 samples. J. Air Waste Manag. Assoc. 68, 494–510.

Cisek, M., Makuch, P., Petelski, T., 2017. Comparison of meteorological conditions in Svalbard fjords: Hornsund and Kongsfjorden. Oceanologia 59, 413–421.

Darani, K.K., Mozafari, M.R., 2010. Supercritical fluids technology in bioprocess industries: a review. J. Biochem. Technol. 2, 144–152.

Duan, J., Tao, J., Wu, Y., Cheng, T., Zhang, R., Wang, Y., Zhu, H., Xie, X., Liu, Y., Li, X., 2017. Comparison of aerosol and cloud condensation nuclei between wet and dry seasons in Guangzhou, southern China. Sci. Total Environ. 607, 11–22.

Eleftheriadis, K., Vratolis, S., Nyeki, S., 2009. Aerosol black carbon in the European arctic: measurements at Zeppelin station, Ny-Ålesund, Svalbard from 1998–2007. Geophys. Res. Lett. 36.

Engelstaedter, S., Washington, R., 2007. Temporal controls on global dust emissions: the role of surface gustiness. Geophys. Res. Lett. 34.

Engvall, A.-C., Krejci, R., Ström, J., Treffeisen, R., Scheele, R., Hermansen, O., Paatero, J., 2008. Changes in Aerosol Properties during Spring-Summer Period in the Arctic Troposphere.

Feingold, G., 2003. Modeling of the first indirect effect: analysis of measurement requirements. Geophys. Res. Lett. 30.

Fisher, J.A., Jacob, D.J., Wang, Q., Bahreini, R., Carouge, C.C., Cubison, M.J., Dibb, J.E., Diehl, T., Jimenez, J.L., Leibensperger, E.M., 2011. Sources, distribution, and acidity of sulfate–ammonium aerosol in the Arctic in winter–spring. Atmos. Environ. 45, 7301–7318.

Freud, E., Krejci, R., Tunved, P., Leaitch, R., Nguyen, Q.T., Massling, A., Skov, H., Barrie, L., 2017. Pan-Arctic aerosol number size distributions: seasonality and transport patterns. Atmos. Chem. Phys. 17.

Georgoulias, A.K., Marinou, E., Tsekeri, A., Proestakis, E., Akritidis, D., Alexandri, G., Zanis, P., Balis, D., Marenco, F., Tesche, M., 2020. A first case study of CCN concentrations from spaceborne lidar observations. Rem. Sens. 12, 1557.

Giardi, F., Becagli, S., Traversi, R., Frosini, D., Severi, M., Caiazzo, L., Ancillotti, C., Cappelletti, D., Moroni, B., Grotti, M., 2016. Size distribution and ion composition of aerosol collected at Ny-Ålesund in the spring–summer field campaign 2013. Rendiconti Lincei 27, 47–58.

Glantz, P., Tesche, M., 2012. Assessment of two aerosol optical thickness retrieval algorithms applied to MODIS Aqua and Terra measurements in Europe. Atmos. Meas. Tech. 5, 1727–1740.

Gong, S., Zhao, T., Sharma, S., Toom-Sauntry, D., Lavoué, D., Zhang, X., Leaitch, W., Barrie, L., 2010. Identification of trends and interannual variability of sulfate and black carbon in the Canadian High Arctic: 1981–2007. J. Geophys. Res.: Atmospheres 115.

Grandey, B., Stier, P., Wagner, T., 2013. Investigating relationships between aerosol optical depth and cloud fraction using satellite, aerosol reanalysis and general circulation model data. Atmos. Chem. Phys. 13, 3177–3184.

Graßl, S., 2019. Properties of Arctic Aerosols Based on Photometer Long-Term Measurements in Ny-Ålesund.

Graßl, S., Ritter, C., 2019. Properties of arctic aerosol based on sun photometer long-term measurements in Ny-Ålesund, Svalbard. Rem. Sens. 11, 1362.

Gutman, G., Reissell, A., 2011. Eurasian Arctic Land Cover and Land Use in a Changing Climate. Springer.

Hallberg, A., Ogren, J., Noone, K., Okada, K., Heintzenberg, J., Svenningsson, I., 1994. The influence of aerosol particle composition on cloud droplet formation. J. Atmos. Chem. 19, 153–171.

Herenz, P., Wex, H., Henning, S., Kristensen, T.B., Rubach, F., Roth, A., Borrmann, S., Bozem, H., Schulz, H., Stratmann, F., 2018. Measurements of aerosol and CCN properties in the Mackenzie River delta (Canadian Arctic) during spring–summer transition in May 2014. Atmos. Chem. Phys. 18, 4477.

Hopper, J., Worthy, D., Barrie, L., Trivett, N., 1994. Atmospheric observations of aerosol black carbon, carbon dioxide and methane in the high Arctic. Atmos. Environ. 28, 3047–3054.
Hubanks, P., Platnick, S., King, M., Ridgway, B., 2015. MODIS Atmosphere L3 Gridded Product Algorithm Theoretical Basis Document (Atbd) & Users Guide. ATBD Reference Number ATBDMOD-30, NASA 125.
Hudson, J.G., Noble, S., Jha, V., 2011. On the relative role of sea salt cloud condensation nuclei (CCN). J. Atmos. Chem. 68, 71–88.
Jacob, D.J., Crawford, J., Maring, H., Clarke, A., Dibb, J.E., Emmons, L., Ferrare, R., Hostetler, C., Russell, P., Singh, H., 2010. The Arctic Research of the Composition of the Troposphere from Aircraft and Satellites (ARCTAS) Mission: Design, Execution, and First Results.
Jayachandran, V.N., Suresh Babu, S.N., Vaishya, A., Gogoi, M.M., Nair, V.S., Satheesh, S. K., Krishna Moorthy, K., 2020. Altitude profiles of cloud condensation nuclei characteristics across the Indo-Gangetic Plain prior to the onset of the Indian summer monsoon. Atmos. Chem. Phys. 20, 561–576.
Jefferson, A., 2010. Empirical estimates of CCN from aerosol optical properties at four remote sites. Atmos. Chem. Phys. 10, 6855–6861.
Jung, C.H., Yoon, Y.J., Kang, H.J., Gim, Y., Lee, B.Y., Ström, J., Krejci, R., Tunved, P., 2018. The seasonal characteristics of cloud condensation nuclei (CCN) in the arctic lower troposphere. Tellus B 70, 1–13.
Kapustin, V., Clarke, A., Shinozuka, Y., Howell, S., Brekhovskikh, V., Nakajima, T., Higurashi, A., 2006. On the determination of a cloud condensation nuclei from satellite: challenges and possibilities. J. Geophys. Res.: Atmospheres 111.
King, M.D., Menzel, W.P., Kaufman, Y.J., Tanré, D., Gao, B.-C., Platnick, S., Ackerman, S. A., Remer, L.A., Pincus, R., Hubanks, P.A., 2003. Cloud and aerosol properties, precipitable water, and profiles of temperature and water vapor from MODIS. IEEE Trans. Geosci. Rem. Sens. 41, 442–458.
Koike, M., Ukita, J., Ström, J., Tunved, P., Shiobara, M., Vitale, V., Lupi, A., Baumgardner, D., Ritter, C., Hermansen, O., 2019. Year-round in situ measurements of Arctic low-level clouds: microphysical properties and their relationships with aerosols. J. Geophys. Res.: Atmospheres 124, 1798–1822.
Konwar, M., Maheskumar, R., Kulkarni, J., Freud, E., Goswami, B., Rosenfeld, D., 2012. Aerosol control on depth of warm rain in convective clouds. J. Geophys. Res.: Atmospheres 117.
Kristjánsson, J.E., 2002. Studies of the aerosol indirect effect from sulfate and black carbon aerosols. J. Geophys. Res.: Atmospheres 107. AAC 1-1-AAC 1-19.
Lance, S., Nenes, A., Medina, J., Smith, J., 2006. Mapping the operation of the DMT continuous flow CCN counter. Aerosol. Sci. Technol. 40, 242–254.
Lathem, T., Beyersdorf, A., Thornhill, K., Winstead, E., Cubison, M., Hecobian, A., Jimenez, J., Weber, R., Anderson, B., Nenes, A., 2013. Analysis of CCN activity of Arctic aerosol and Canadian biomass burning during summer 2008. Atmos. Chem. Phys. 13, 2735–2756.
Li, K., Ye, X., Pang, H., Lu, X., Chen, H., Wang, X., Yang, X., Chen, J., Chen, Y., 2018. Temporal variations in the hygroscopicity and mixing state of black carbon aerosols in a polluted megacity area. Atmos. Chem. Phys. 18, 15201–15218.
Liu, D., Allan, J., Whitehead, J., Young, D., Flynn, M., Coe, H., McFiggans, G., Fleming, Z. L., Bandy, B., 2013. Ambient black carbon particle hygroscopic properties controlled by mixing state and composition. Atmos. Chem. Phys. 13, 2015–2029.
Liu, S., Aiken, A.C., Gorkowski, K., Dubey, M.K., Cappa, C.D., Williams, L.R., Herndon, S. C., Massoli, P., Fortner, E.C., Chhabra, P.S., 2015. Enhanced light absorption by mixed source black and brown carbon particles in UK winter. Nat. Commun. 6, 1–10.
Liu, J., Li, Z., 2014. Estimation of cloud condensation nuclei concentration from aerosol optical quantities: influential factors and uncertainties. Atmos. Chem. Phys. 14.
Liu, J., Zheng, Y., Li, Z., Cribb, M., 2011. Analysis of cloud condensation nuclei properties at a polluted site in southeastern China during the AMF-China Campaign. J. Geophys. Res.: Atmospheres 116.
Lund Myhre, C., Nielsen, C., 2004. Optical properties in the UV and visible spectral region of organic acids relevant to tropospheric aerosols. Atmos. Chem. Phys. 4, 1759–1769.
Ma, X., Bartlett, K., Harmon, K., Yu, F., 2013. Comparison of AOD between CALIPSO and MODIS: significant differences over major dust and biomass burning regions. Atmos. Meas. Tech. 6, 2391.
Mahowald, N., Albani, S., Kok, J.F., Engelstaeder, S., Scanza, R., Ward, D.S., Flanner, M. G., 2014. The size distribution of desert dust aerosols and its impact on the Earth system. Aeolian Res. 15, 53–71.
Mamouri, R.-E., Ansmann, A., 2016. Potential of polarization lidar to provide profiles of CCN-and INP-relevant aerosol parameters. Atmos. Chem. Phys. 16, 5905–5931.
Maskey, S., Chong, K.Y., Seo, A., Park, M., Lee, K., Park, K., 2017. Cloud condensation nuclei activation of internally mixed black carbon particles. Aerosol Air Qual. Res. 17, 867–877.
Matsuki, A., Quennehen, B., Schwarzenboeck, A., Crumeyrolle, S., Venzac, H., Laj, P., Gomes, L., 2010. Temporal and vertical variations of aerosol physical and chemical properties over West Africa: AMMA aircraft campaign in summer 2006. Atmos. Chem. Phys. 10, 8437–8451.
Matsumoto, K., Tanaka, H., Nagao, I., Ishizaka, Y., 1997. Contribution of particulate sulfate and organic carbon to cloud condensation nuclei in the marine atmosphere. Geophys. Res. Lett. 24, 655–658.
McCoy, D., Bender, F.M., Mohrmann, J., Hartmann, D., Wood, R., Grosvenor, D., 2017. The global aerosol-cloud first indirect effect estimated using MODIS, MERRA, and AeroCom. J. Geophys. Res.: Atmospheres 122, 1779–1796.
McMeeking, G., Good, N., Petters, M., McFiggans, G., Coe, H., 2011. Influences on the fraction of hydrophobic and hydrophilic black carbon in the atmosphere. Atmos. Chem. Phys. 11, 5099–5112.
Menon, S., Saxena, V., Durkee, P., Wenny, B., Nielsen, K., 2002. Role of sulfate aerosols in modifying the cloud albedo: a closure experiment. Atmos. Res. 61, 169–187.
Moore, R., Bahreini, R., Brock, C., Froyd, K., Cozic, J., Holloway, J., Middlebrook, A., Murphy, D., Nenes, A., 2011. Hygroscopicity and composition of Alaskan arctic CCN during April 2008. Atmos. Chem. Phys. Discuss. 11.
Moosmüller, H., Chakrabarty, R., Arnott, W., 2009. Aerosol light absorption and its measurement: a review. J. Quant. Spectrosc. Radiat. Transf. 110, 844–878.
Nair, V.S., Jayachandran, V.N., Kompalli, S.K., Gogoi, M.M., Babu, S.S., 2020. Cloud condensation nuclei properties of South Asian outflow over the northern Indian Ocean during winter. Atmos. Chem. Phys. 20, 3135–3149.
Nakajima, T., Higurashi, A., Kawamoto, K., Penner, J.E., 2001. A possible correlation between satellite-derived cloud and aerosol microphysical parameters. Geophys. Res. Lett. 28, 1171–1174.
Penna, B., Herdies, D., Costa, S., 2018. Estimates of direct radiative forcing due to aerosols from the MERRA-2 reanalysis over the Amazon region. Atmos. Chem. Phys. Discuss. 1–17.
Penner, J.E., Andreae, M., Annegarn, H., Barrie, L., Feichter, J., Hegg, D., Jayaraman, A., Leaitch, R., Murphy, D., Nganga, J., 2001. Aerosols, Their Direct and Indirect Effects, Climate Change 2001: the Scientific Basis. Contribution of Working Group I to the Third Assessment Report of the Intergovernmental Panel on Climate Change. Cambridge University Press, pp. 289–348.
Perring, A.E., Schwarz, J.P., Markovic, M.Z., Fahey, D.W., Jimenez, J.L., Campuzano-Jost, P., Palm, B.D., Wisthaler, A., Mikoviny, T., Diskin, G., 2017. In situ measurements of water uptake by black carbon-containing aerosol in wildfire plumes. J. Geophys. Res.: Atmospheres 122, 1086–1097.
Pierce, J., Adams, P., 2009. Uncertainty in global CCN concentrations from uncertain aerosol nucleation and primary emission rates. Atmos. Chem. Phys. 9.
Quaas, J., Ming, Y., Menon, S., Takemura, T., Wang, M., Penner, J.E., Gettelman, A., Lohmann, U., Bellouin, N., Boucher, O., 2009. Aerosol indirect effects–general circulation model intercomparison and evaluation with satellite data. Atmos. Chem. Phys. 9, 8697–8717.
Raatikainen, T., Brus, D., Hyvärinen, A.-P., Svensson, J., Asmi, E., Lihavainen, H., 2015. Black carbon concentrations and mixing state in the Finnish Arctic. Atmos. Chem. Phys. 15, 10057–10070.
Randles, C., Da Silva, A., Buchard, V., Colarco, P., Darmenov, A., Govindaraju, R., Smirnov, A., Holben, B., Ferrare, R., Hair, J., 2017. The MERRA-2 aerosol reanalysis, 1980 onward. Part I: system description and data assimilation evaluation. J. Clim. 30, 6823–6850.
Rastak, N., Silvergren, S., Zieger, P., Wideqvist, U., Ström, J., Svenningsson, B., Maturilli, M., Tesche, M., Ekman, A.M., Tunved, P., 2014. Seasonal variation of aerosol water uptake and its impact on the direct radiative effect at Ny-Ålesund, Svalbard. Atmos. Chem. Phys. 14, 7445–7460.
Remer, L.A., Kaufman, Y., Tanré, D., Mattoo, S., Chu, D., Martins, J.V., Li, R.-R., Ichoku, C., Levy, R., Kleidman, R., 2005. The MODIS aerosol algorithm, products, and validation. J. Atmos. Sci. 62, 947–973.
Rodríguez, E., Toledano, C., Cachorro, V., Ortiz, P., Stebel, K., Berjón, A., Blindheim, S., Gausa, M., de Frutos, A., 2012. Aerosol characterization at the sub-Arctic site Andenes (69° N, 16° E), by the analysis of columnar optical properties. Q. J. R. Meteorol. Soc. 138, 471–482.
Romakkaniemi, S., Arola, A., Kokkola, H., Birmili, W., Tuch, T., Kerminen, V.M., Räisänen, P., Smith, J., Korhonen, H., Laaksonen, A., 2012. Effect of aerosol size distribution changes on AOD, CCN and cloud droplet concentration: case studies from Erfurt and Melpitz, Germany. J. Geophys. Res.: Atmospheres 117.
Salomonson, V.V., Barnes, W., Maymon, P.W., Montgomery, H.E., Ostrow, H., 1989. MODIS: Advanced facility instrument for studies of the Earth as a system. IEEE Trans. Geosci. Rem. Sens. 27, 145–153.
Schmeisser, L., Backman, J., Ogren, J.A., Andrews, E., Asmi, E., Starkweather, S., Uttal, T., Fiebig, M., Sharma, S., Eleftheriadis, K., 2018. Seasonality of Aerosol Optical Properties in the Arctic.
Schwarz, J., Samset, B., Perring, A., Spackman, J., Gao, R., Stier, P., Schulz, M., Moore, F., Ray, E.A., Fahey, D., 2013. Global-scale seasonally resolved black carbon vertical profiles over the Pacific. Geophys. Res. Lett. 40, 5542–5547.
Sharma, S., Lavoué, D., Cachier, H., Barrie, L., Gong, S., 2004. Long-term trends of the black carbon concentrations in the Canadian Arctic. J. Geophys. Res.: Atmospheres 109.
Shinozuka, Y., Clarke, A., DeCarlo, P., Jimenez, J., Dunlea, E., Roberts, G., Tomlinson, J., Collins, D., Howell, S., Kapustin, V., 2009. Aerosol Optical Properties Relevant to Regional Remote Sensing of CCN Activity and Links to Their Organic Mass Fraction: Airborne Observations over Central Mexico and the US West Coast during MILAGRO/INTEX-B. 1foldr Import 2019-10-08 Batch 9.
Shinozuka, Y., Clarke, A.D., Nenes, A., Jefferson, A., Wood, R., McNaughton, C.S., Ström, J., Tunved, P., Redemann, J., Thornhill, K.L., 2015. The relationship between cloud condensation nuclei (CCN) concentration and light extinction of dried particles: indications of underlying aerosol processes and implications for satellite-based CCN estimates. Atmos. Chem. Phys. 15, 7585–7604.
Springston, S., 2018. Particle Soot Absorption Photometer (PSAP) Instrument Handbook. DOE ARM Climate Research Facility, Washington, DC, USA.
Stier, P., 2016. Limitations of passive remote sensing to constrain global cloud condensation nuclei. Atmos. Chem. Phys. 16, 6595–6607.
Stocker, T., 2014. Climate Change 2013: the Physical Science Basis: Working Group I Contribution to the Fifth Assessment Report of the Intergovernmental Panel on Climate Change. Cambridge university press.
Stohl, A., 2006. Characteristics of atmospheric transport into the Arctic troposphere. J. Geophys. Res.: Atmospheres 111.
Ström, J., Engvall, A.C., Delbart, F., Krejci, R., Treffeisen, R., 2009. On small particles in the Arctic summer boundary layer: observations at two different heights near Ny-Ålesund, Svalbard. Tellus B: Chem. Phys. Meteorol. 61, 473–482.

Ström, J., Umegård, J., Tørseth, K., Tunved, P., Hansson, H.-C., Holmén, K., Wismann, V., Herber, A., König-Langlo, G., 2003. One year of particle size distribution and aerosol chemical composition measurements at the Zeppelin Station, Svalbard, March 2000–March 2001. Phys. Chem. Earth 1181–1190. Parts A/B/C 28.

Tang, J., Wang, P., Mickley, L.J., Xia, X., Liao, H., Yue, X., Sun, L., Xia, J., 2014. Positive relationship between liquid cloud droplet effective radius and aerosol optical depth over Eastern China from satellite data. Atmos. Environ. 84, 244–253.

Tao, W., Li, X., Khain, A., Matsui, T., Lang, S., Simpson, J., Chen, J.-P., Li, Z., Wang, C., Zhang, C., 2012. Impact of aerosols on convective clouds and precipitation. Rev. Geophys. 50.

Teinilä, K., Hillamo, R., Kerminen, V.-M., Beine, H., 2004. Chemistry and modal parameters of major ionic aerosol components during the NICE campaigns at two altitudes. Atmos. Environ. 38, 1481–1490.

Tunved, P., Ström, J., Krejci, R., 2013. Arctic aerosol life cycle: linking aerosol size distributions observed between 2000 and 2010 with air mass transport and precipitation at Zeppelin station, Ny-Å lesund, Svalbard. Atmos. Chem. Phys. 13.

Wang, Q., Jacob, D.J., Fisher, J.A., Mao, J., Leibensperger, E., Carouge, C., Le Sager, P., Kondo, Y., Jimenez, J., Cubison, M., 2011. Sources of Carbonaceous Aerosols and Deposited Black Carbon in the Arctic in Winter-Spring: Implications for Radiative Forcing.

Wang, Y., Wang, J., Levy, R.C., Xu, X., Reid, J.S., 2017. MODIS retrieval of aerosol optical depth over turbid coastal water. Rem. Sens. 9, 595.

Weber, R., Lee, S., Chen, G., Wang, B., Kapustin, V., Moore, K., Clarke, A., Mauldin, L., Kosciuch, E., Cantrell, C., 2003. New particle formation in anthropogenic plumes advecting from Asia observed during TRACE-P. J. Geophys. Res.: Atmospheres 108.

Yuan, T., Li, Z., Zhang, R., Fan, J., 2008. Increase of cloud droplet size with aerosol optical depth: an observation and modeling study. J. Geophys. Res.: Atmospheres 113.

Zábori, J., Rastak, N., Yoon, Y., Riipinen, I., Ström, J., 2015. Size-resolved cloud condensation nuclei concentration measurements in the Arctic: two case studies from the summer of 2008. Atmos. Chem. Phys. Discuss. 15.

Zhang, J., Liu, J., Tao, S., Ban-Weiss, G., 2015. Long-range transport of black carbon to the Pacific Ocean and its dependence on aging timescale. Atmos. Chem. Phys. 15, 11521–11535.

Zhang, A., Wang, Y., Zhang, Y., Weber, R.J., Song, Y., Ke, Z., Zou, Y., 2020. Modeling the global radiative effect of brown carbon: a potentially larger heating source in the tropical free troposphere than black carbon. Atmos. Chem. Phys. 20, 1901–1920.

Zhou, J., Swietlicki, E., Berg, O.H., Aalto, P.P., Hämeri, K., Nilsson, E.D., Leck, C., 2001. Hygroscopic properties of aerosol particles over the central Arctic Ocean during summer. J. Geophys. Res.: Atmospheres 106, 32111–32123.